10 (2022) 100107

Contents lists available at ScienceDirect

Biosensors and Bioelectronics: X

journal homepage: www.journals.elsevier.com/biosensors-and-bioelectronics-x

Flexible sensing devices integrating molecularly-imprinted polymers for the detection of 3-nitrotyrosine biomarker

G.V. Martins [a,b,c,*], A. Riveiro [d], S. Chiussi [d], M.G.F. Sales [a,b,c]

[a] BioMark@ISEP, School of Engineering of Polytechnique School of Porto, 4200-072, Porto, Portugal
[b] BioMark@UC, Department of Chemical Engineering, Coimbra University, 3030-790, Coimbra, Portugal
[c] CEB, Centre of Biological Engineering, University of Minho, 4710-057, Braga, Portugal
[d] CINTECX, Universidade de Vigo, Vigo, Spain

ARTICLE INFO

Keywords:
Molecularly-imprinted polymer
Flexible substrate
Gold-based electrodes
Electrochemical (bio)sensor
Oxidative stress biomarker

ABSTRACT

In recent years, the development of flexible and wearable devices for healthcare and biomedical applications has become an emerging technological goal, particularly with personalized medicine on the rise. As a response to the increasing demand for *in-situ* sensing platforms that fulfil some essential requirements like sensitivity, reproducibility and high stability, electrochemical sensors have boosted their way for innovative approaches. So, high-quality flexible sensing strategies are still a demand for local monitoring.

Herein, a flexible three-electrode system was fabricated on transparent polymeric sheet substrate through physical deposition of gold as working, counter, and reference electrodes. Along the fabrication process, the electrochemical performance of these electrodes was assessed by means of cyclic voltammetry (CV) while gold adherence to the plastic material was continuously improved. Afterwards, a high-performance molecularly-imprinted sensing film inspired by natural recognition mechanism was assembled through electropolymerization of phenol monomer, in the presence of 3-nitrotyrosine (3-NT), directly on the gold surface. Under the optimized conditions, the flexible (bio)sensor platform was able to detect the presence of 3-NT over the concentration range 10 pg/mL – 1 μg/mL, enabling one of the lower limits of detection found in the literature (1.13 pg/mL or 24.9 pM). The obtained (bio)sensor displayed good reproducibility, stability and selectivity over the chosen interfering substances.

Overall, the developed electrochemical device may serve as a flexible, miniaturized, and reliable platform, with potential to be applied in the future as wearable sensing technology.

1. Introduction

Flexible skin-like devices are gaining increasing attention in the field of implantable and wearable sensors targeted for human health applications to enable *point-of-care* (POC) monitoring in a non-invasive way (Bai et al., 2018). Under this perspective, skin-like sensors are being envisioned as artificial extensions of human's natural sensors that includes visual, touch, olfactory, auditory and taste sensors. Although there have been major breakthroughs in the development of this novel technology, the integration of biosensing features with high quality flexible devices is still an emerging need. The real challenge of designing a bendable and flexible electronic device is highly dependent of the kind of substrates as well as active materials, polymeric or inorganic, that can be selected for each particular application (Yin et al., 2010). Currently, the most popular flexible sensors are designed for the assessment of important biological parameters, like, pH (Guinovart et al., 2014), temperature (Moser and Gijs, 2007), pressure (Santos et al., 2018), glucose levels (Jankowska et al., 2017), among others. Besides the obvious functionality of the device directly assembled at the site of interest, enabling more surface contact points also, the flexible structure of these electrodes avoids some of the problems related to the rigid one, such as, easy damage of electrodes as well as less probability of cracking during the process of fabrication and storage (Liu et al., 2014). Thus, simple, efficient, and flexible electronic systems are highly promising to be incorporated in continuous, quick, and low-cost sensing platforms.

Over the last years, miniaturized devices also known as *lab-on-a-chip* (LOC) have received great attention due to their ability to accomplish laboratory analysis at small scale (Ibarlucea et al., 2016; Nguyen et al.,

* Corresponding author. BioMark@ISEP. School of Engineering of Polytechnique School of Porto, 4200-072, Porto, Portugal.
E-mail address: fvm.gabriela@gmail.com (G.V. Martins).

https://doi.org/10.1016/j.biosx.2022.100107
Received 19 November 2021; Received in revised form 30 December 2021; Accepted 5 January 2022
Available online 13 January 2022
2590-1370/© 2022 The Author(s). Published by Elsevier B.V. This is an open access article under the CC BY license (http://creativecommons.org/licenses/by/4.0/).

2018). The main features of these compact platforms include handling small sample with volumes and enabling quick diagnostic outputs. Therefore, in order to overcome the main limitations of the three-electrode conventional design, screen-printed electrodes (SPEs) have appeared as stable, fast and disposable tools for the detection of a wide range of target molecules in medical diagnostics, environmental, food and pharmaceutical analyses (Hughes et al., 2016; Yamanaka et al., 2016). In addition, the small arrangement of SPEs have allowed important characteristics from an analytical point-of-view, such as, portability and miniaturization (Bartsch et al., 2019). These single-use electrochemical devices are often based on the application of conductive inks directly into robust and rigid substrates, allowing the analysis of a small drop of few microliters. Regarding the fabrication of sensitive electrochemical sensors on plastic substrates, simple methods, like for instance, wax patterning, hand-painting and drop casting had been widely explored but, often with the need to incorporate nanostructured materials to achieve sufficient or better electrochemical performance (Carneiro et al., 2018; Chen et al., 2019). Meanwhile, the use of alternative materials over the conventional stiff supports, like for instance, cellulose and textile, is emerging in order to accomplish compatible, sustainable, inexpensive and bendable devices with potential to be employed for *in-situ* real-time monitoring (Economou et al., 2018; Liu and Lillehoj, 2017; Tang et al., 2019) (Kongkaew et al., 2021) (Costa-Rama and Fernández-Abedul, 2021).

In this context, the development of mechanically flexible and highly sensitive sensors for the detection of relevant biological markers can be helpful for diagnosis and follow-up of various diseases. In particular, (bio)sensors have been widely explored in the field of healthcare monitoring due to their ease and quick fabrication, low-cost, simple operation and portability (Maduraiveeran et al., 2017). One of the most common ways to finely design the bio-recognition element responsible for the selective and sensitive response of the sensor is by using a molecular imprinting technique. Molecularly imprinted polymers (MIPs) are known for their high stability and resistance against degradation, low cost and simple fabrication procedures (Cieplak and Kutner, 2016). Briefly, MIPs are described as synthetic polymers designed with specific recognition sites that are complementary in size, shape and functional groups to the target molecule (Sergey and Anthony, 2006). Over the last years, these artificial recognition materials have been successfully coupled to different nano-structured materials, like, carbon dots (Karfa et al., 2016), carbon nanotubes (Khan et al., 2016), gold nanoparticles (Huang et al., 2011) and magnetic nanoparticles (Sedghi et al., 2018), for conductivity enhancement and signal amplification purposes.

Herein, the main goal of this work is to describe the fabrication of a novel flexible gold electrode holding high stability and reproducibility features to be used in POC applications (Fig. 1). In this, the electrodes are assembled by a single conductive material and, consequently one single mask-step, resulting in a much simpler and less costly methodology compared to the conventional ones. In addition, the use of pure gold in the assembly of the 3-eletrode system renders more sensitive and reproducible electrochemical devices. As proof-of-concept, the gold-based electrodes were employed in the production of a novel biosensing system for 3-nitrotyrosine (3-NT), a well-established oxidative-stress biomarker and relevant predictor of disease progression (Kanyong et al., 2020). It has been acknowledged that formation of 3-NT is directly correlated with aging (Syslová et al., 2014), chronic inflammation (Conventz et al., 2007), diabetes (Simsek et al., 2015), cardiovascular (Daiber and Münzel, 2012), neurodegenerative (Ahsan, 2013) and

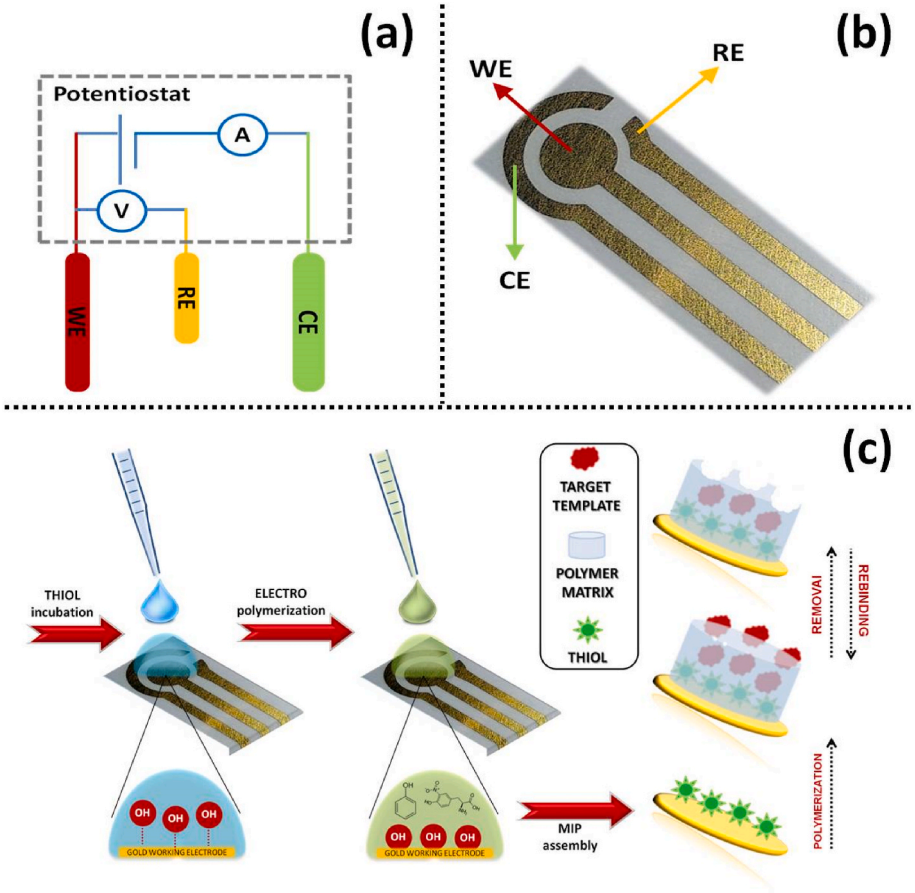

Fig. 1. Schematic illustration of (a) an analytical three-electrode potentiostat setup, (b) the fabricated gold-based electrode (WE, CE, and RE are the working, counter, and reference electrode, respectively) and (c) the assembly of the MIP film on the surface of the flexible electrodes. (For interpretation of the references to colour in this figure legend, the reader is referred to the Web version of this article.)

cancer (Rossi et al., 2009) pathologies.

Up to now, there are already some variety of biosensing systems for the detection and quantification of 3-NT (Table 1) but most of them are still highly dependent of the inclusion of nanostructured materials for amplification purposes (Varodi et al., 2020). Besides increasing the cost and complexity of the fabrication procedure, these methodologies are still far from enabling a reproducible and costly miniaturized device to be implemented in POC context. Moreover, a previous work of our group (Martins et al., 2020) has presented the construction of a paper-based MIP sensor for the detection of 3-NT with good selectivity and sensitivity features. Nevertheless, the obtained limit of detection (LOD) was higher, and the cellulose substrate holds some limitations in terms of flexibility and robustness for a reliable POC use. Herein, the comparison of the proposed sensor with others employed for 3-NT determination shows that our (bio)sensor coated on the flexible gold electrodes presented a better analytical performance, enabling a detection limit down to picoMolar level, the lower value found with electrochemical detection. Furthermore, the only sensor for 3-NT detection found with a better LOD was accomplished by using Surface Plasmon Resonance (SPR), which constitutes a considerable limitation to be applied in POC analysis due to cost and miniaturization issues. Thus, this work describes the production of an integrated 3-electrodes system based on gold conductive material supported in transparent flexible polymer sheets. Afterwards, a MIP nanolayer was tailored *in-situ* at the surface of the gold-electrode as a way to introduce the selective biomimetic element into the final set-up. These electrodes were continuously optimized and characterized, to undergo suitable optimized procedure, as a way to achieve high stability, reproducibility and selectivity performance.

2. Materials and methods

2.1. Reagents

All reagents and solution preparation are detailed in **Supplementary Information**.

2.2. Fabrication of improved gold-based electrodes

Herein, transparent flexible polymer sheets were employed as the substrate for the fabrication of advanced flexible electrodes holding high purity gold (Au) surfaces. Flexible Polyethylene Naphthalate (PEN) (Teonex, Teijin DuPont) sheets were used as substrate materials, because they are already widely employed as highly transparent substrate material in optical and optoelectronic applications. They also undergo reduced thermal shrinkage (0.1% at 200 °C for 10 min), which allowed using higher temperature steps, if required. The PEN sheets where further roughened by using abrasive paper and coated with Au in a Physical Vapour Deposition (PVD) system (10^{-2} mPa base pressure) via thermal evaporation of 99,99% purity Au (K.Lesker). The procedure is provided in **Supplementary Information**.

2.3. Characterization of the gold-based electrodes

The techniques and parameters used for the characterization of the electrodes are described in **Supplementary Information**.

2.4. Electrochemical assays

The electrochemical performance of the gold-based 3-electrodes was investigated by means of cyclic voltammetry (CV). These electrodes were electrochemically characterized by a potentiostat/galvanostat from Metrohm Autolab (PGSTAT302N with an FRA module), through a suitable interface switch box and controlled by ANOVA software. Before each experiment, the electrode area was precisely defined with hot glue and all the presented potential values are related to the gold pseudo-reference of the electrodes. The full description of the electrochemical measurements is included in the **Supplementary Information**.

2.5. Assembly of the MIP film

Before use, the bare gold electrodes were cleaned by washing with a

Table 1
Comparison of the analytical properties of different sensors for 3-nitrotyrosine detection.

Method	Nature of the substrate	Biorecognition element	Flexible platform	Analytical performance	References
SPR detection	Au	Antibody	NO	LR 0.028–4.8 μg/mL (LOD 4.7 ng/mL)	Jin et al. (2011)
HPLC detection with SPE	–	MIP	NO	LR 2.5–55 μg/mL (LOD 0.7 μg/mL)	Mergola et al. (2013)
Electrochemical detection	Bimetallic Fe/Pd nanoparticles	MIP	NO	LR 4.90–867.57 μg/L (LOD 1.20 μg/L)	Roy et al. (2015)
SPR detection	Graphene	–	NO	LR 0.5–1000 pg/mL (LOD 0.13 pg/mL)	Ng et al. (2016)
Luminescent detection	Binuclear Pt (pca) (bpy) doped sol-gel	–	NO	LR $1.85x10^{-5}$–$7.95x10^{-10}$ mol/L (LOD 10.47 nM)	Attia and Al-Radadi (2016)
Fluorescent detection	Carbon dots	MIP	NO	LR 0.050–1.85 μM (LOD 17 nM)	Jalili and Amjadi (2018)
Electrochemical detection	GCE electrode with AuNPs	MIP	NO	LR 0.2–50.0 μM (LOD 50.0 nM)	Wang et al. (2018)
Electrochemical detection	$CdWO_4$ ND@RGO modified SPEs	–	NO	LR 18.5nM-1.84 mM (LOD 3.24 nM)	Govindasamy et al. (2018)
Electrochemical detection	$CuFe_2O_4$@RGO composite	–	NO	LR 4.25 nM-1347.5 μM (LOD 25.14 pM)	Chen et al. (2018)
Electrochemical detection	Glassy carbon electrode	–	NO	LR 0.05–30.0 μM (LOD 17.0 nM)	Zhai et al. (2019)
Luminescent detection	AuNCs@ZIF-8 composites	–	NO	LR of 5–200 nM (LOD 1.8 nM)	Jalili et al. (2020)
Electrochemical detection	Carbon-coated paper substrate	MIP	NO	LR 500 nM-1 mM (LOD 22.3 nM)	Martins et al. (2020)
HPLC separation + electrochemical detection	–	–	NO	LR 10–500 nM (LOD 10 nM)	Vujacic-Mirski et al. (2020)
Electrochemical detection	ZrO_2@rGO composites on GCE	–	NO	LR0.025–855.2 μM (LOD 9 nM)	Maheshwaran et al. (2020)
Electrochemical detection	Bimetallic Pd/Au thin film electrodes	–	NO	LR 0.002–30 μmol/L (LOD 2 nM)	Ju et al. (2020)
Electrochemical detection	***Gold-based electrodes***	***MIP***	***YES***	***LR 10 pg/mL - 1 μg/mL (LOD 1.13 pg/mL or 24.9 pM)***	***This work***

AuNCs@ZIF-8: gold nanoclusters into zeolitic-imidazolate frameworks-8; AuNPs: gold nanoparticles; bpy: bipyridine; $CdWO_4$: cadmium tungstate; $CuFe_2O_4$@RGO: copper ferrite nanodots entrapped in reduced graphene oxide nanosheets; Fe: iron; GCE: glass carbon electrode; HPLC: High Performance Liquid Chromatography; LR: Linear Range; LOD: Limit of Detection; MIP: molecular imprinting polymer; ND@RGO: nanodots decorated reduced graphene oxide; pca: 2-pyrazinecarboxylic acid; Pd:palladium; Pt: platinum; SPEs: screen-printed electrodes; SPR: Surface Plasmon Resonance; ZrO_2@rGO: nanostructured zirconia on reduced graphene oxide.

99% ethanolic solution for approximately 30 s, rinsing abundantly with ultra-pure water and drying with nitrogen. Initially, the Au surface of the electrodes was modified with a monolayer of 3-mercapto-1-hexanol. The clean Au electrode was immersed in a 20 mM thiol solution for 90 min, at 25 °C, to form the covalent attachment of thiol to the Au electrode surface. This incubation step was responsible for the formation of a stable self-assembled monolayer (SAM) on the electrode surface through a strong gold-sulphur interaction.

The electropolymerization of phenol monomer was performed by CV (3 cycles) in the potential range +0.20 to +0.70 V, at a scan rate of 20 mV/s, in phosphate buffer solution at 7.0 pH, in the presence and absence of the template molecule 3-NT. Afterwards, this template was removed by consecutive immersion in 0.5 M H_2SO_4 solution and water, for 30 min each, leading to the formation of recognition cavities in the MIP structure.

Control electrodes (NIPs or non-imprinted polymer) were prepared by following the same procedure but without the presence of the template molecule. The NIP electrode had the same treatment as the MIP sensor, to ensure that variations were only attributed to the imprinting features. All experiments were carried out at ambient temperature. Finally, the modified electrodes were (wet) stored at 4 °C before further use.

2.6. Selectivity assays

Selectivity experiments were carried out through incubation on the MIP-based sensor of a 3-NT solution (4 ng/mL) with or without selected interfering species, with similar concentrations. Herein, uric acid, creatinine, tyrosine, tryptophan, glycine and ascorbic acid were selected as interfering molecules, because they co-exist with 3-NT in biological fluids or/and can exhibit electro-active properties.

3. Results and discussion

3.1. Fabrication of flexible gold electrodes

Along the development of our MIP sensing device with improved sensitivity, an important task included the fabrication and optimization of advanced flexible electrodes. A more detailed discussion regarding the manufacturing process is provided in **Supplementary Information**.

In a first approach, Au electrodes shapes were aimed to be like conventional commercial SPEs with a 4 mm diameter working electrode (Fig. 2 a.b), although different configurations should be easily fabricated through the same procedure. Afterwards, electrodes with Au thickness of 10–400 nm, as corroborated by a stylus profiler, were fabricated and evaluated, showing that a thickness of 200 nm was sufficient to ensure a good electrical contact/measurement. Herein, the area of the working electrode was 13 mm^2, with a counter electrode at 1 mm distance, as determined by optical profiler (Fig. 2c). Furthermore, these results showed the flexibility of the electrodes which had an ability to withstand pressure and avoid damage as no obvious change was found before and after bending course of the electrode, from visual observation and electrical performance.

While the polymer sheets were easy to clean and dry, the adherence of Au films to this substrate material was only satisfactory, i.e. endure wiping with ethanol soaked tissue, for thin films (<100 nm) deposited on the side of PEN (*Teonex Q65*FA) sheets that were treated in factory for enhanced performance. However, increasing film thickness above 100 nm led to a deterioration of adherence not always passing simple "scotch-tape" peel tests.

In order to improve the adherence of Au films on glass and polymer surfaces several techniques are known, such as, plasma treatment, wet chemistry functionalization with thiol groups or deposition of intermediate Chromium (Cr) or Titanium (Ti) adhesion layers, surface

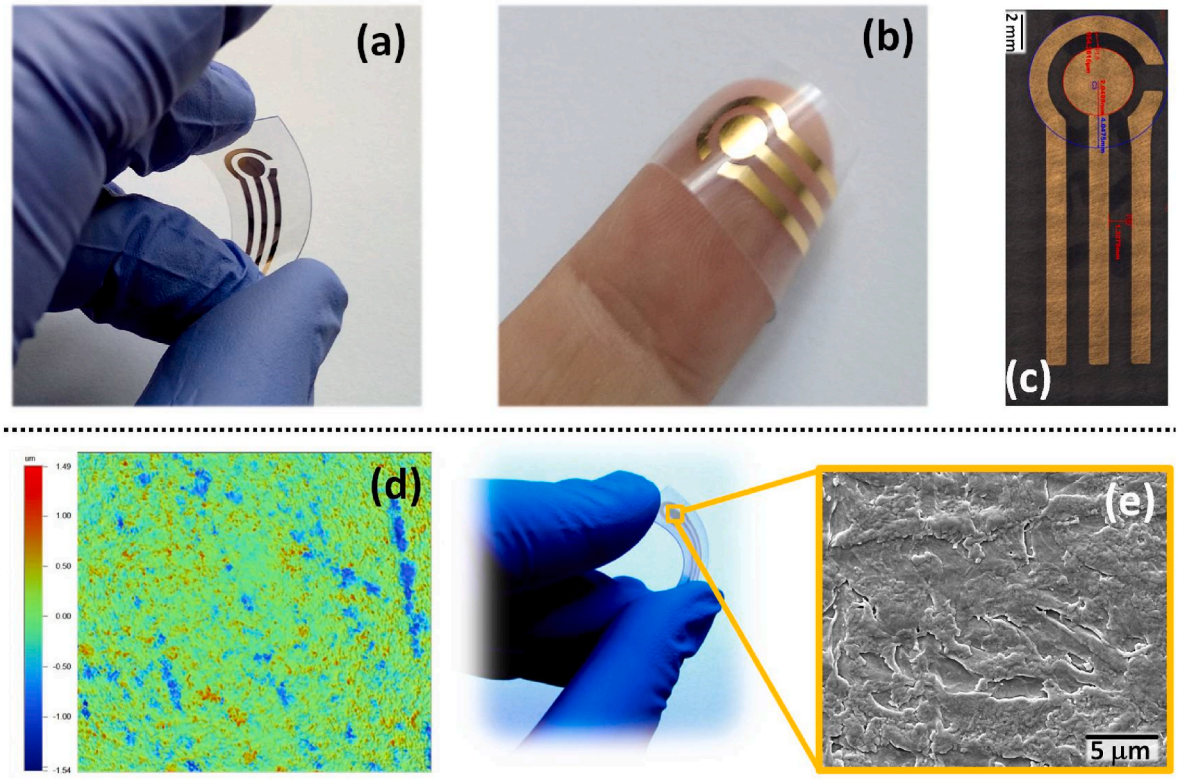

Fig. 2. (a–b) Photos of flexible and bendable Au electrodes on surface roughened PEN with (c) dimensions of the electrodes. Size of the working electrode was of 13 mm^2, with a counter electrode of 4 mm external radius at 1 mm distance. (d) Typical 2-D image of the 3-D interferometric profiler analysis for an Au surface on a flexible PEN surface roughened with 12 µm abrasive paper and (e) SEM image of the surface of the gold working electrode (10000× magnification). (For interpretation of the references to colour in this figure legend, the reader is referred to the Web version of this article.)

roughening, and complex multilayer structures among others (Li et al., 2004; Moazzez et al., 2013; Neděla et al., 2016; Sidler et al., 2008). Since fast and economic processes were aimed, the effects of simple mechanical roughening with abrasive paper were investigated. Herein, abrasive paper with 5 μm, 12 μm, 30 μm and 46 μm grain size was used that led to root mean square surface roughness (Sq) values of (0,23 ±5%) μm, (0,30 ±10%) μm, (1,2 ±0,1) μm and (1,6 ±0,2) μm, respectively. These values were obtained analysing the 3-D surface roughness imaged of a 227 × 298 μm^2 region with an optical interferometric profiler, as can be seen in Fig. 2d.

While treating with an abrasive sheet of lowest grain size (5 μm) did not show any improvement of adherence, compared to the original sheet exhibiting an Sq of (0,003 ± 5%) μm, all other roughened surfaces efficiently fix up to 400 nm thick Au films that resist all applied cleaning procedures, such as resolute scrubbing with organic solvent-soaked tissues and ultra-sonic bath treatment. So, for further studies the surface sample roughened with the lowest grain size was discarded. Also, the surface morphology of the fabricated gold electrode was further characterized by SEM (Fig. 2e), where a relatively smooth surface was observed, with slight cracks and a visible finer uniform roughness, which constitutes an evidence that surface homogeneity was preserved.

Overall, this "roughening" effect in the surface of substrates is not restricted to the need of adherence's enhancement. It can be also applied as a strategy to improve the performance of the electrodes by increasing the area of the electrochemically active surface without changing the geometric surface of the electrodes. Furthermore, in some cases, this "manual treatment" can be by itself a considerable influence regarding the reproducibility of the electrodes. So, in order to ensure a reproducible cleaning process, it is necessary to determine and check for certain properties regarding the final gold surface. Along this study, imaging techniques such as AFM micrographs or SEM photographs were used to check and confirm the reproducibility of the surface treatment procedure by measuring the surface roughness for different batches. The standard variation was around 5–10%, thereby considering that the system offers as it is suitable reproducibility.

3.2. Electrochemical performance evaluation

CV is the most commonly employed electrochemical technique in order to study the reduction and oxidation processes, as well as electron transfer-initiated chemical reactions that take place at the electrode surface (Elgrishi et al., 2018). Herein, the electrochemical characteristics of the different gold-based electrodes were investigated by means of CV in a solution composed by a redox specie and a supporting electrolyte. The main conclusions are provided in the **Supplementary Information.** Briefly, our results demonstrated that the electrochemical processes follow the Randles-Sevcik equation for a diffusion-controlled reaction at the electrode surface, in the chosen experimental conditions (Fig. S1). In addition, the presented data have shown that all the tested electrodes displayed an electro-active area higher in comparison with their respective geometric area. PEN Q65FA 12 μm grain electrodes were also selected for further studies as they were the only ones that enabled a higher value of active surface area against the respective value obtained with commercial gold-SPEs from DropSens.

3.3. Development of a biosensor for 3-NT

3.3.1. Assembly of MIP material

In this work, phenol was selected among various monomers holding suitable characteristics to be used in the fabrication of MIP films and enabling in this case the formation of intermolecular interactions between 3-NT and phenol units. These interactions are essentially important for the formation of the imprinted cavities, as they are responsible for the subsequent recognition of 3-NT. These are likely to involve π interactions between the aromatic rings and hydrogen bridges between O/N and H atoms in both phenol and 3-NT.

The polyphenol polymeric network was obtained by *in-situ* electropolymerization of phenol in the presence of 3-NT. Electropolymerization enables quick and easy formation of a biorecognition layer directly on a conductive substrate, as gold. Herein, the introduction of a thiol coating (3-mercapto-1-hexanol) on the gold-based working electrode conferred a greater stability during the assembly of the polymeric film, an evidence that has already been observed in previous studies (Xie et al., 2010) (Martins et al., 2016). After, MIP films were obtained by electropolymerizing phenol in a phosphate buffer solution of 100 mM at a pH of 7.0 containing 3-NT molecule.

3.3.1.1. Monomer electropolymerization. Firstly, it was necessary to select the most suitable potential window to promote the formation of a stable and robust layer of poly (phenol) without causing damage or any alteration to the imprinted molecule. Typical cyclic voltammograms of individual solutions of phenol, 3-NT and phosphate buffer are presented in Fig. 3a. As expected, pure phenol solution exhibited only an oxidation peak, around +0.60 V, indicating that the oxidation of the monomer is of irreversible nature. In addition, 3-NT exhibited a broad anodic peak around +0.90 V which is a strong indication that under these conditions it displays electroactive behaviour. So, to avoid that the template structure changes electrochemically while the polymer is growing around it, a narrow potential range of (+0.2 V to +0.70 V) was chosen.

As the number of scans increased, a significant decrease in the peak current was observed, revealing the formation of a non-conductive polymer layer (Fig. 3b). Besides the initial current values, no significant difference was observed between the cyclic voltammograms obtained during the electropolymerization in the presence or absence of 3-NT (MIP and NIP, respectively), because it is not electroactive in this condition. The number of cycles applied was also optimized, with 3-cycles giving more stable and reproducible electrochemical responses, without a great increase in the overall resistance of the sensing layer.

3.3.1.2. Template removal. The removal of the 3-NT molecules entrapped within the polymeric network is required for the generation of imprinted cavities on the polymeric matrix, with complementary size and shape to the original molecule. Along with the proper efficacy to remove the template, there is also the need that the polymeric matrix keeps its structure, without suffering damage or degradation. Therefore, different washing approaches were tested in both NIP and MIP-modified electrodes that included ethanolic or acidic solutions. Overall, the use of a solution of 0.5 M of sulphuric acid (30 min of incubation at room temperature) was considered the best approach for template removal to ensure an efficient removal of 3-NT.

The electrochemical properties of the electrodes obtained after each modification step were characterized by electrochemical impedance spectroscopy (EIS) measurements in 5 mM $[Fe(CN)_6]^{3-/4-}$ solution prepared in 100 mM of phosphate buffer, and the results are illustrated in Fig. 3c. The typical spectrum includes a semicircle related to charge transfer resistance (Rct) and a linear part signalling diffusion (Muñoz et al., 2017). The EIS data obtained herein did not evidence diffusion and were fitted with a Randle's equivalent circuit consisting of electrolyte resistance (Rs), the capacitance element (Cd), and Rct. Thus, the Rct value was related to the semicircle size and it is the element of the circuit that best describes the resistance to charge-transfer of the redox species at the electrode surface. After the formation of the thiol monolayer on the gold electrodes, it was observed an increase in the Rct values from <50 Ω (clean gold) to 450 Ω, as the result of a higher obstruction to the electron transfer kinetics of the redox-probe at the electrode interface. Afterwards, as expected, the introduction of the poly (phenol) film at the surface of the electrode resulted in a substantial increase of impedance, with the MIP sensor displaying a stronger insulating behaviour in comparison with the NIP.

After template removal, it was observed that both NIP and MIP showed decreasing Rct values. The non-imprinted sensors exhibited a

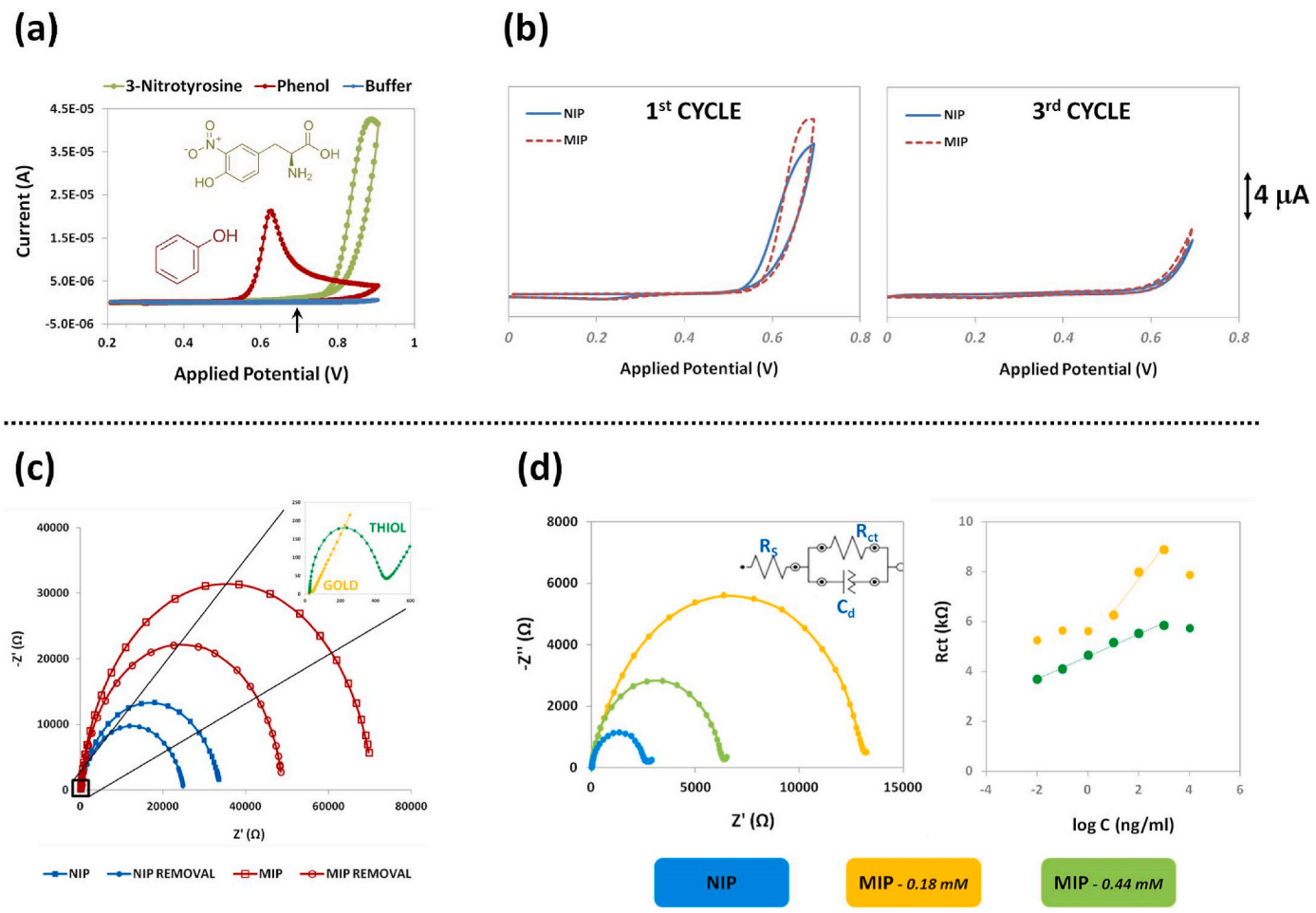

Fig. 3. (a) Cyclic voltammograms of individual solutions (prepared in 100 mM of phosphate buffer solution, pH 7.2) of phenol, 3-nitrotyrosine and only phosphate buffer, at a scan rate of 20 mV/s, for one cycle. (b) Cyclic voltammograms for the electropolymerization of 0.30 mM phenol in 100 mM of phosphate buffer, pH 7.0, (scan rate 20 mV/s) at gold-modified electrodes with (dashed line) and without (straight line) the template molecule 3-NT for the first cycle and third cycle. (c) EIS curves of thiol-modified electrode NIP (blue line) and MIP (red line) before (circle symbol) and after (square symbol) template removal (inset figure with gold and thiol-modified electrodes), measured in aqueous solution containing 5 mM $[Fe(CN)_6]^{3-/4-}$ in 100 mM of phosphate buffer at pH 7.0 (d) Nyquist plots obtained for NIP and MIP materials (inset is the equivalent circuit applied) and calibration curves regarding the MIPs response after 3-NT rebinding. (For interpretation of the references to colour in this figure legend, the reader is referred to the Web version of this article.)

reduced impedance of ~25%, whereas the imprinted sensors led to a decrease by 30–45% in the same conditions. Although the effect of the removal step is more pronounced for the MIP material, some variation also occurred in the NIP material that can be justified due to the washout of unreacted monomer or even some structural rearrangement. Any structural rearrangement of these groups during the removal step may also contribute to conformational changes around the binding cavities formed in the MIP material, which may enable the release of the imprinted molecules. Such structural rearrangement is more likely to occur at the exposed surface of the polymer than at the imprinted cavities, as these are first protected by the imprinted molecule that needs to the removed. Besides, any structural rearrangement of the MIP sensor can also enhance the porosity of the polymeric matrix which can result in an easy diffusional pathway of the analyte to the cavities.

3.3.1.3. Monomer/template ratio. Herein, the concentration ratio of the monomer (phenol) to the imprinted molecule (3-NT) during the electropolymerization step was optimized since it influences the performance/response of the (bio)sensor by controlling the thickness of the polymer film, the stability of the polymeric network and the number of recognition sites created. In theory, the binding positions of the MIP are higher for higher 3-NT concentrations, but the stability of the polymer is typically better for higher concentrations of monomer. In addition, polyphenol is a non-conducive material and higher concentrations of phenol may lead to increased resistances, which in turn my hinder sensitivity.

The effect of the monomer/template ratio study was followed by EIS measurements in 5 mM $[Fe(CN)_6]^{3-/4-}$ solution, prepared in 100 mM of phosphate buffer. To this end, two different concentrations of 3-NT were investigated during phenol electropolymerization, one higher (0.44 mM) and another lower (0.18 mM) than the monomer concentration (0.3 mM). The effect of these ratios was investigated by binding different 3-NT concentrations and plotting the Rct values of a standard iron redox probe against the logarithmic concentration. Our results have showed that the presence of the template molecule in the polyphenol matrix hindered the electron transfer process on the electrode surface, resulting in higher Rct values in comparison with the NIP ones (Fig. 3d). Moreover, it was noticed that a lower concentration of template molecules entrapped in the polymeric film is responsible for a higher increase in the Rct value, meaning that for higher concentration of 3-NT the growth of the film can also become limited. Afterwards, an optimum response was achieved for the MIP assembled in the conditions using a superior concentration of 3-NT, which could be explained due to a higher number of rebinding sites available in the surface. In addition, in the case of the lower concentration of 3-NT, the linear range of response was much narrower and only responded for higher concentrations of 3-NT. Thus, in

further studies it was used a template concentration of 0.44 mM.

3.4. Analytical performance of the (bio)sensor and regeneration of the gold surface

3.4.1. Calibration curve

Under optimal conditions, the quantitative determination of 3-NT using the modified gold electrodes was investigated by means of EIS. Before the rebinding assay, the stability of the sensing film was established by performing successive incubations in phosphate buffer solution, for 30 min, until the Rct value presents a variation less than 5% (RSD). Fig. S2 illustrates different electrodes prepared in different days, during the buffer incubation step until a stable Rct signal was reached. Afterwards, the Rct increased with the increasing 3-NT concentration (Fig. 4a.b) because of the binding of 3-NT molecules to the imprinted sites, thereby blocking the sites available for the $[Fe(CN)_6]^{3-/4-}$ probe to access the electrode surface. Accordingly, the Rct value was proportionally increased as the logarithm of 3-NT concentration in solution was increased. As can be seen in Fig. 4c, a linear tendency was obtained for both imprinted and non-imprinted materials over the log 3-NT concentration range 10 pg/mL – 1 μg/mL, but the MIP sensor showed higher sensitivity (slope = 0.1136, abscissa = 1.2714) and better linearity (r^2 = 0.9861) in comparison with the NIP (slope = 0.0753, abscissa = 1.1546). The limit of detection (LOD) was calculated using IUPAC protocol (LOD=3σ/slope) and it turned out to be 1.13 pg/mL (24.9 pM), where σ concerns the standard deviation of blank measurements. Moreover, the reproducibility of the (bio)sensor was investigated over the entire linear range and the results showed that the relative standard deviation (RSD) was less than 10% for the MIPs. In contrast, the NIP curve presented a lower sensitivity and a higher standard deviation for each standard solution reading.

3.4.2. Selectivity assays

The selectivity of the proposed (bio)sensor constitutes a crucial criterion to grant its successful application. Herein, uric acid, tyrosine, creatinine, tryptophan, glycine and ascorbic acid were selected as interfering species. EIS measurements were performed after incubation of the MIP-based sensor in single 3-NT solution (4 ng/mL) and in an equimolar mixture with each interfering species. Each interferent assay was performed in triplicate and all RSD were <10%. Data presented in Fig. 5 confirmed that these interfering species had negligible effect upon the reading of 3-NT. The analytical changes observed corresponded to −2.5%, −5.1%, −5.1%, −7.2%, +1.5% and −8.6% for uric acid, tyrosine, creatinine, tryptophan, glycine and ascorbic acid respectively. As shown in Fig. 5, the response of the (bio)sensor was not significantly affected by the addition of the interfering substances compared with pure 3-NT solution and, among all tested compounds, tryptophan and ascorbic acid presented the highest interference.

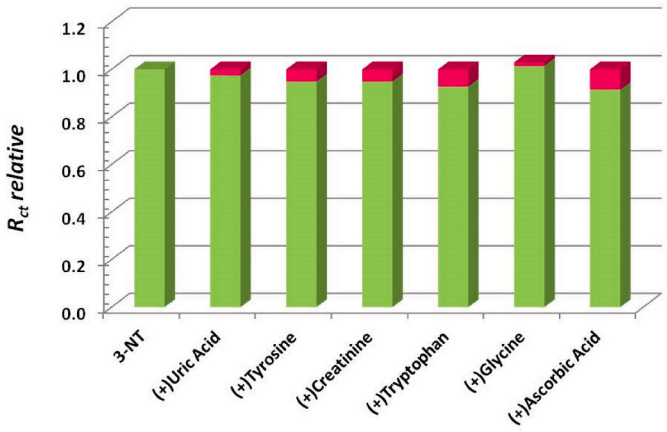

Fig. 5. EIS measurement of MIP-based sensor recorded after incubation in 4 ng/ml 3-NT solution, alone and in the presence of equimolar quantities of uric acid, creatinine, tyrosine, tryptophan, glycine and ascorbic acid. All solutions were prepared freshly in phosphate buffer solution (100 mM, pH 7.0).

3.4.3. Reusing the flexible gold electrodes

The optimized cleaning procedure and the obtained data are discussed in **Supplementary Information**.

4. Conclusions

In this work, improved gold-based electrodes have been successfully used as flexible electrical platforms for the assembly of sensitive molecularly-imprinted electrochemical sensor aimed for 3-NT detection. The fabrication process of the electrodes constitutes a simple, fast and straightforward approach, holding a great potential to be in the future translated through up-scalable processes. These electrodes offer beneficial electrochemical features when compared to others prepared by screen-printing techniques and employing gold inks.

Afterwards, the integration of the molecular imprinting technology directly in the electrode surface results in a synthetic recognition element capable of selective detection of 3-NT biomarker. During the MIP synthesis, experimental parameters like monomer-template ratio and removal of the imprinted molecule were optimized and the ability of the proposed sensor to selectively rebind the target was demonstrated. In sum, the imprinted-based (bio)sensor displayed high electrochemical performance on the detection of 3-NT biomarker over the concentration range 10 pg/mL to 1 μg/mL and one of the lowest LODs found in the literature. Moreover, the developed (bio)sensor showed good reproducibility, high stability, quick response and suitable selectivity performance.

Overall, this innovative sensing system provides a potential route for the fabrication of *in-situ* diagnosis sensing devices with the ability to

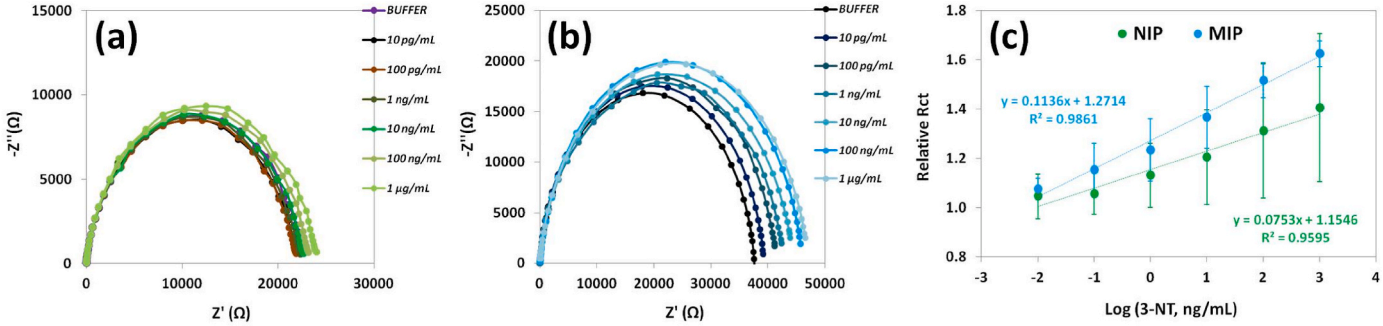

Fig. 4. Nyquist plot of (a) NIP and (b) MIP sensors in 5 mM $[Fe(CN)_6]^{3-/4-}$ in 100 mM of phosphate buffer solution at pH 7.0, previously incubated in increasing concentrations of 3-NT; (c) corresponding calibration curves for both NIP and MIP sensors. All error bars represent the standard deviation for three independent measurements.

withstand mechanical deformation, without compromising their electrochemical performance.

CRediT authorship contribution statement

G.V. Martins: Conceptualization, Methodology, Writing – original draft. **A. Riveiro:** Methodology, Investigation. **S. Chiussi:** Methodology, Visualization, Investigation. **M.G.F. Sales:** Supervision, Validation, Writing – review & editing.

Declaration of competing interest

The authors declare that they have no known competing financial interests or personal relationships that could have appeared to influence the work reported in this paper.

Acknowledgments

The authors acknowledge the financial support from IBEROS project (Instituto de Bioingeniería en Red para el Envejecimiento Saludable, INTERREG POCTEP/0245_IBEROS_1_E) supported by FEDER, also within the cooperation region of Galicia/Spain and North of Portugal, and the Portuguese Foundation for Science and Technology (FCT) under the scope of the strategic funding of PEst UIDB/04469/2020 unit.

Appendix A. Supplementary data

Supplementary data to this article can be found online at https://doi.org/10.1016/j.biosx.2022.100107.

References

Ahsan, H., 2013. Hum. Immunol. 74, 1392–1399.
Attia, M.S., Al-Radadi, N.S., 2016. Biosens. Bioelectron. 86, 406–412.
Bai, W., Kuang, T., Chitrakar, C., Yang, R., Li, S., Zhu, D., Chang, L., 2018. Biosens. Bioelectron. 122, 189–204.
Bartsch, H., Peipmann, R., Himmerlich, M., Müller, J., Bund, A., Witte, H., 2019. Prog. Org. Coating 135, 545–554.
Carneiro, M.C.C.G., Moreira, F.T.C., Dutra, R.A.F., Fernandes, R., Sales, M.G.F., 2018. Microchem. J. 138, 35–44.
Chen, S., Qamar, A.Z., Asefifeyzabadi, N., Funneman, M., Taki, M., Elliot, L., Kinsel, M.E., Kinsel, G.R., Shamsi, M.H., 2019. Sci. Rep. 9, 6131.
Chen, S.M., Umamaheswari, R., Mani, G., Chen, T.W., Ali, M.A., Fahad, A.H., Elshikh, M. S., Farah, M.A., 2018. Inorg. Chem. Front. 5, 944–950.
Cieplak, M., Kutner, W., 2016. Trends Biotechnol. 34, 922–941.
Conventz, A., Musiol, A., Brodowsky, C., Müller-Lux, A., Dewes, P., Kraus, T., Schettgen, T., 2007. J. Chromatogr. B Anal. Technol. Biomed. Life Sci. 860, 78–85.
Costa-Rama, E., Fernández-Abedul, M.T., 2021. Biosensors 11, 1–23.
Daiber, A., Münzel, T., 2012. Circulation 126, 2371–2373.
Economou, A., Kokkinos, C., Prodromidis, M., 2018. Lab Chip 18, 1812–1830.
Elgrishi, N., Rountree, K.J., McCarthy, B.D., Rountree, E.S., Eisenhart, T.T., Dempsey, J. L., 2018. J. Chem. Educ. 95, 197–206.
Govindasamy, M., Manavalan, S., Chen, S.M., Umamaheswari, R., Chen, T.W., 2018. Sensor. Actuator. B Chem. 272, 274–281.
Guinovart, T., Valdés-Ramírez, G., Windmiller, J.R., Andrade, F.J., Wang, J., 2014. Electroanalysis 26, 1345–1353.
Huang, J., Xing, X., Zhang, X., He, X., Lin, Q., Lian, W., Zhu, H., 2011. Food Res. Int. 44, 276–281.
Hughes, G., Westmacott, K., Honeychurch, K.C., Crew, A., Pemberton, R.M., Hart, J.P., 2016. Biosensors 6, 1–39.
Ibarlucea, B., Munoz-Berbel, X., Ortiz, P., Büttgenbach, S., Fernández-Sánchez, C., Llobera, A., 2016. Sensor. Actuator. B Chem. 237, 16–23.
Jalili, R., Amjadi, M., 2018. Sensor. Actuator. B Chem. 255, 1072–1078.
Jalili, R., Dastborhan, M., Chenaghlou, S., Khataee, A., 2020. J. Photochem. Photobiol. Chem. 391, 112370.
Jankowska, D.A., Bannwarth, M.B., Schulenburg, C., Faccio, G., Maniura-Weber, K., Rossi, R.M., Scherer, L., Richter, M., Boesel, L.F., 2017. Biosens. Bioelectron. 87, 312–319.
Jin, J., Wang, C., Tao, Y., Tan, Y., Yang, D., Gu, Y., Deng, H., Bai, Y., Lu, H., Wan, Y., 2011. Sensor. Actuator. B Chem. 153, 164–169.
Ju, J., Liu, X., Yu, J.-J., Sun, K., Fathi, F., Zeng, X., 2020. Anal. Chem. 92, 6538–6547.
Kanyong, P., Patil, A.V., Davis, J.J., 2020. Annu. Rev. Anal. Chem. 13, 183–200.
Karfa, P., Roy, E., Patra, S., Kumar, D., Madhuri, R., Sharma, P.K., 2016. Biosens. Bioelectron. 78, 454–463.
Khan, M.A.R., Moreira, F.T.C., Riu, J., Sales, M.G.F., 2016. Sensor. Actuator. B Chem. 233, 697–704.
Kongkaew, S., Kanatharana, P., Thavarungkul, P., Limbut, W., 2021. J. Colloid Interface Sci. 583, 487–498.
Li, W.T., Charters, R.B., Luther-Davies, B., Mar, L., 2004. Appl. Surf. Sci. 233, 227–233.
Liu, J., Lu, C.Y., Zhou, H., Xu, J.J., Chen, H.Y., 2014. ACS Appl. Mater. Interfaces 6, 20137–20143.
Liu, X., Lillehoj, P.B., 2017. Biosens. Bioelectron. 98, 189–194.
Maduraiveeran, G., Sasidharan, M., Ganesan, V., 2017. Biosens. Bioelectron. 103, 113–129.
Maheshwaran, S., Akilarasan, M., Chen, S.-M., Chen, T.-W., Tamilalagan, E., Tzu, C.Y., Lou, B.-S., 2020. J. Electrochem. Soc. 167, 066517.
Martins, G.V., Marques, A.C., Fortunato, E., Sales, M.G.F., 2020. Sens. Bio-Sens. Res. 28, 100333.
Martins, G.V., Marques, A.C., Fortunato, E., Sales, M.G.F., 2016. Biosens. Bioelectron. 86, 225–234.
Mergola, L., Scorrano, S., Del Sole, R., Lazzoi, M.R., Vasapollo, G., 2013. Biosens. Bioelectron. 40, 336–341.
Moazzez, B., O'Brien, S.M., Merschrod, E.F.S., 2013. Sensors 13, 7021–7032.
Moser, Y., Gijs, M.A.M., 2007. J. Microelectromech. Syst. 16, 2279–2282.
Muñoz, J., Montes, R., Baeza, M., 2017. Trends Anal. Chem. 97, 201–215.
Neděla, O., Slepička, P., Kolská, Z., Slepičková Kasálková, N., Sajdl, P., Veselý, M., Švorčík, V., 2016. React. Funct. Polym. 100, 44–52.
Ng, S.P., Qiu, G., Ding, N., Lu, X., Wu, C.-M.L., 2016. Biosens. Bioelectron. 89, 468–476.
Nguyen, T., Andreasen, S.Z., Wolff, A., Bang, D.D., 2018. Micromachines 9, 1–12.
Rossi, T. De, Panis, C., Victorino, V.J., De, L.F., Cristina, A., Cecchini, A.L., 2009. Appl. Canc. Res. 29, 150–156.
Roy, E., Patra, S., Madhuri, R., Sharma, P.K., 2015. Talanta 132, 406–415.
Santos, A. dos, Pinela, N., Alves, P., Santos, R., Fortunato, E., Martins, R., Águas, H., Igreja, R., 2018. Proceedings 2, 1039.
Sedghi, R., Yassari, M., Heidari, B., 2018. Colloids Surf. B Biointerfaces 162, 154–162.
Sergey, P., Anthony, T., 2006. Molecular Imprinting of Polymers. Landes Bioscience.
Sidler, K., Vazquez-Mena, O., Savu, V., Villanueva, G., van den Boogaart, M.A.F., Brugger, J., 2008. Microelectron. Eng. 85, 1108–1111.
Simsek, S., Stam, F., ten Boekel, E., ter Wee, M.M., Krul-Poel, Y.H.M., van Wijland, H., Westra, S., Lips, P.T.A.M., van Schoor, N.M., 2015. Diabetes Care 38, 1420–1426.
Syslová, K., Böhmová, A., Mikoška, M., Kuzma, M., Pelclová, D., I, P.K., 2014. Oxid. Med. Cell. Longev. 2014, 1–14.
Tang, R.H., Liu, L.N., Zhang, S.F., He, X.C., Li, X.J., Xu, F., Ni, Y.H., 2019. Microchim. Acta 186, 1–25.
Varodi, C., Pogacean, F., Gheorghe, M., Mirel, V., Coros, M., Barbu-Tudoran, L., van Staden, R.I.S., Pruneanu, S., 2020. Sensors 20, 1–13.
Vujacic-Mirski, K., Bruns, K., Kalinovic, S., Oelze, M., Kröller-Schön, S., Steven, S., Mojovic, M., Korac, B., Münzel, T., Daiber, A., 2020. Antioxidants 9, 1–21.
Wang, S., Sun, G., Chen, Z., Liang, Y., Zhou, Q., Pan, Y., Zhai, H., 2018. Electrochim. Acta 259, 893–902.
Xie, C., Li, H., Li, S., Wu, J., Zhang, Z., 2010. Anal. Chem. 82, 241–249.
Yamanaka, K., Vestergaard, M.C., Tamiya, E., 2016. Sensors 16, 1–16.
Yin, Z.P., Huang, Y.A., Bu, N. Bin, Wang, X.M., Xiong, Y.L., 2010. Chin. Sci. Bull. 55, 3383–3407.
Zhai, H., Wang, S., Zhou, J., Pan, J., Tong, Y., Mei, Q., Zhou, Q., 2019. J. Electrochem. Soc. 166, B1426–B1433.